

Disentangling Subpopulations in Single-Molecule FRET and ALEX Experiments with Photon Distribution Analysis

Toma E. Tomov, Roman Tsukanov, Rula Masoud, Miran Liber, Noa Plavner, and Eyal Nir*

Department of Chemistry, Ben-Gurion University of the Negev, Be'er-Sheva, Israel

ABSTRACT Among the advantages of the single-molecule approach when used to study biomolecular structural dynamics and interaction is its ability to distinguish between and independently observe minor subpopulations. In a single-molecule Förster resonance energy transfer (FRET) and alternating laser excitation diffusion experiment, the various populations are apparent in the resultant histograms. However, because histograms are calculated based on the per-burst mean FRET and stoichiometry ratio and not on the internal photon distribution, much of the acquired information is lost, thereby reducing the capabilities of the method. Here we suggest what to our knowledge is a novel statistical analysis tool that significantly enhances these capabilities, and we use it to identify and isolate static and dynamic subpopulations. Based on a kernel density estimator and a proper photon distribution analysis, for each individual burst, we calculate scores that reflect properties of interest. Specifically, we determine the FRET efficiency and brightness ratio distributions and use them to reveal 1), the underlying structure of a two-state DNA-hairpin and a DNA hairpin that is bound to DNA origami; 2), a minor doubly labeled dsDNA subpopulation concealed in a larger singly labeled dsDNA; and 3), functioning DNA origami motors concealed within a larger subpopulation of defective motors. Altogether, these findings demonstrate the usefulness of the proposed approach. The method was developed and tested using simulations, its rationality is described, and a computer algorithm is provided.

INTRODUCTION

Single-molecule fluorescence techniques (1) are used regularly to address a variety of biological questions involving nano-sized biomolecules such as DNA (2), DNA nanostructures (3–6), proteins (7–10), and their interactions (11,12). The observation of single molecules enables the structural dynamics and molecular interactions of a species of interest to be investigated even in the presence of a greater heterogeneous ensemble. Moreover, the fluorescent basis of the method enables in situ examinations in the preferable aqueous environment.

Generally speaking, samples are either surface-bound or freely diffusing in the solution. In the latter case, the subject of this work, picomolar concentrations of fluorescently labeled samples stochastically diffuse into and out of a confocal spot, resulting in sequential absorption and emission, from which anywhere from a few dozen to a few thousand photons, collectively called a “burst”, are recorded. In a typical single-molecule Förster resonance energy transfer (smFRET) experiment, a single laser directly excites the donor dye, and, depending on donor-acceptor distance, energy is transferred to the acceptor dye via the FRET process. The FRET efficiency of each burst is analyzed by dividing the number of detected acceptor photons into that

of all the photons, regardless of their distribution in the burst (or by analyzing the donor and acceptor excited electronic state lifetimes (13), a method not discussed here). The FRET efficiencies of many bursts are then plotted in a histogram that reflects the sample static and dynamic heterogeneities, and the photon statistic, called “shot-noise”. In an extended experimental scheme, called alternating laser excitation (ALEX (14) or PIE (15)), two or three (16,17) lasers (two- or three-color ALEX, respectively), each directly exciting a corresponding dye, alternate. Here dye stoichiometry or brightness ratio is calculated for each burst by dividing the number of photons recorded during the time periods when the donor-laser is on into the overall number of photons, as in FRET, regardless of their distribution in the burst. This method enables dye stoichiometry to be measured for affinity or integrity measurements and enables the removal of donor-only, acceptor-only, and mixed subpopulations. The resultant FRET/ALEX values are placed in a two-dimensional histogram that is then interpreted.

Although some structurally related biomolecular questions can be answered by measuring the mean FRET efficiency and observing its change in response to changing conditions or different samples, the solutions to other questions require a detailed understanding of structural dynamics. Because FRET histograms reflect molecular dynamics, an attempt has been made in recent years to describe the relationship between molecular dynamics and the resultant FRET histogram. Semiempirical statistical descriptions of shot-noise contribution to histogram shape and width have been developed (18–20), yielding excellent agreement between modeled and simulated histograms.

Submitted August 1, 2011, and accepted for publication November 21, 2011.

*Correspondence: eyalnir@bgu.ac.il

This is an Open Access article distributed under the terms of the Creative Commons-Attribution Noncommercial License (<http://creativecommons.org/licenses/by-nc/2.0/>), which permits unrestricted noncommercial use, distribution, and reproduction in any medium, provided the original work is properly cited.

Editor: David Millar.

© 2012 by the Biophysical Society
0006-3495/12/03/1163/11 \$2.00

doi: 10.1016/j.bpj.2011.11.4025

To incorporate dynamics, methods to calculate or simulate the expected mean FRET efficiency distribution for a two-state system (19,21–23) or for every given system (24,25) were recently developed. Although these methods use information from the photon distribution, it remains limited, thus causing the loss of information stored in the photon distribution and decreasing the applicability of this approach.

We postulate that the photon distributions inside the various channels contain information that can be exploited to achieve several significant experimental and analytical improvements. We suggest taking the following approach: A statistical analysis based on photon arrival times is conducted for each burst, resulting in a score that reflects a specific property and that enables the identification and robust and straightforward filtering of subpopulations according to that property.

More specifically, we propose two slightly different functions for estimating the degree of FRET efficiency and brightness ratio distributions in the burst. 1). A FRET-based estimator capable of identifying and partially resolving molecular dynamics. We demonstrate the exposure of the underlying structure of a hairpin and confirm its quasi-two-state behavior. 2). A brightness-based estimator capable of identifying and removing donor-only and acceptor-only subpopulations, subpopulation mixing (26), dye bleaching (27,28), and blinking (29,30) events. We demonstrate the identification of a minor, doubly labeled dsDNA subpopulation hidden in a larger, singly labeled dsDNA subpopulation, and the identification of functioning, intact DNA origami-based motors concealed within a much larger population of defective motors. We carefully describe the statistical method, explain its rationale, demonstrate its validity using numerical simulations, and provide a computer algorithm for its easy implementation.

MATERIAL AND METHODS

Numeric simulations

A detailed description of the simulation is provided in the [Supporting Material](#).

Sample preparation and buffers

For a more detailed description of the preparation methods, see the [Supporting Material](#). In short, the DNA origami follows Rothmund's design for the rectangle with bridged seam (31). The hairpin was introduced into the origami by not introducing one of the DNA staples (r-1t16f) and instead inserting the hairpin's bottom sequence elongated with the r-1t16f sequence (see [Fig. S2](#) in the [Supporting Material](#)). DNA motor footholds (32) were similarly introduced.

Samples were measured at 20 μL of buffer solution that was placed on a KOH-treated coverslip and then sealed with Teflon and another coverslip. The buffer comprised 10 mM Tris-Base pH 8, 1 mM EDTA, 10 $\mu\text{g}/\text{mL}$ bovine serum albumin (Sigma-Aldrich, St. Louis, MO), 1 mM Trolox (33) (Sigma-Aldrich), and 100 mM NaCl for the dsDNA. The hairpin and the origami-hairpin were measured in 250 mM NaCl and 5 mM NaCl, respec-

tively, to achieve ~50:50 distributions between the open and closed states. For the DNA motor, instead of NaCl, 3 mM MgAc was used.

Experimental setup and data analysis

The single-molecule FRET-ALEX experiments were performed, and the experimental and simulated data as described before in Nir et al. (19) with some improvements (see the [Supporting Material](#)).

Burst beginnings and ends were determined using the all-photons-burst search (19). The parameters were: $L = 200$, $M = 10$, and $T = 200 \mu\text{s}$, for the dsDNA and the freely diffusing hairpin, $L = 1000$, $M = 100$, and $T = 2500 \mu\text{s}$ for the origami hairpin, and $L = 200$, $M = 100$, and $T = 2500 \mu\text{s}$ for the origami motor. For the FRET-2CDE we used $\tau = 45 \mu\text{s}$ and for ALEX-2CDE we used $\tau = 75 \mu\text{s}$ unless mentioned otherwise. For each burst, E , S , FRET-2CDE, and ALEX-2CDE were calculated, binned (0.01 bin size), and plotted on a one- or two-dimensional histogram.

THEORY

Let us first reiterate some conventional definitions.

Proximity ratio, FRET efficiency, and E -histogram in single-laser experiments

For reasons of simplicity and reasons explained in the [Supporting Material](#), here we calculate only the experimentally observed FRET value, E , which is commonly defined as the ratio of the number of photons recorded in the acceptor channel to that of the total photons observed,

$$E = PR = \frac{A}{D + A}, \quad (1)$$

where D and A are the number of photons recorded in the donor-channel (CHD) and acceptor-channel (CHA), respectively. Qualitatively, mean E reflects the donor-acceptor mean distance whereas fluctuations in donor-acceptor distance result in fluctuations in E . Therefore, identifying and characterizing these fluctuations can potentially help resolve molecular dynamics.

Stoichiometry, brightness ratio, and E/S histogram in two-color ALEX experiments

In the ALEX scheme (14), two or more lasers alternately excite their respective dyes. [Equation 1](#) holds when just the donor laser is active, but when an additional laser (or lasers) alternates with the donor-laser, E is calculated based on the number of photons recorded during the donor laser on-time, leading to a slightly modified definition,

$$E = \frac{A_{DEX}}{D_{DEX} + A_{DEX}}, \quad (2)$$

where D_{DEX} represents the number of photons recorded in the donor channel and A_{DEX} the number of photons recorded in the acceptor channels just during donor-laser on-time.

As commonly defined in ALEX experiments (14), stoichiometry or brightness ratio (S) is calculated by dividing the sum of the photons recorded in the donor and the acceptor channels during donor laser on-time by the sum of the photons recorded on both channels during donor laser on-time and the photons recorded during both the donor and the acceptor laser on-times,

$$S = \frac{D_{DEX} + A_{DEX}}{D_{DEX} + A_{DEX} + D_{AEX} + A_{AEX}} = \frac{D_{EX}}{D_{EX} + A_{EX}}, \quad (3)$$

where D_{EX} and A_{EX} represent the sums of photons recorded on both CHD and CHA during donor laser and acceptor laser on-times (defined as CHD_{EX} and CHA_{EX}), respectively. According to Eq. 3, $S \approx 1$ represents donor-only, $S \approx 0$ represents acceptor-only, and $S \approx 0.5$ represents population with equal number of donor and acceptor dyes (see the Supporting Material). However, because S is influenced by more than just dye stoichiometry (see the Supporting Material), we consider it an indicator for the observable brightness ratio and not as it is usually defined (14).

Estimators and filters rationale

Here we describe our main intellectual contribution—the two-channel kernel (34)-based density distribution estimator (2CDE) function—and its rationale. For a description of the 2CDE LabVIEW V. 7.1 (National Instruments, Austin, TX) computer algorithm, see Fig. S1.

Requirements for FRET-2CDE

A proper estimator and filter are characterized by their abilities to grade and separate the subjects under examination based on their relevant properties while being minimally influenced by foreign properties and artifacts. Unfortunately, photon distribution (and burst duration and burst intensity, called burst size) is strongly influenced by the fluorophores' stochastic emission and by the molecules' stochastic diffusion into, out-of, and inside the confocal spot. These stochastic factors must be overcome if we are to succeed in designing an estimator sensitive to the experimentally meaningful FRET efficiency (and brightness ratio) distribution.

Therefore, we designed the FRET-2CDE estimator to meet several prerequisites: 1), The estimator should be

sensitive to FRET efficiency distribution. Bursts with fixed underlying FRET efficiency will receive low grades whereas those with a distribution of underlying FRET efficiencies will receive high grades. We do not require the estimator to be sensitive to the rates of fluctuations, only to their amplitudes. 2), The estimator should be minimally influenced by the averaged FRET efficiency. 3, It should be minimally dependent on the overall number of photons (burst size), the burst duration, and the overall photon density. To achieve these goals, we combined several statistical features as described below.

Kernel density estimator

The basic element in our function is the so-called kernel (34) density estimator (KDE), here designed to estimate the density of photons around an individual photon. Accordingly, KDE_{Xi}^Y (Eq. 4) estimates the density of any given channel-Y photons around any given channel-X i^{th} photon ($(CHX)_i$). The local density is estimated by summing the weights given for each of the surrounding channel-Y photons, whereas the weight is the exponent of the negative absolute time interval between the $(CHX)_i$ photon and the $(CHY)_j$ photon divided by τ as schematically explained in Fig. 1:

$$KDE_{Xi}^Y(t_{(CHX)_i}, t_{(CHY)_j}) = \sum_j^{N_{CHY}} \exp \left[-\frac{|t_{(CHX)_i} - t_{(CHY)_j}|}{\tau} \right]. \quad (4)$$

To save CPU time, in practice, we only consider photons that are $5 \times \tau$ time before to $5 \times \tau$ time after the i^{th} arrival time (explained in Fig. S1, but not depicted in Eq. 4). We verified that using longer periods has no significant effect on the results (data not shown).

Correctly estimating the density of channel-X photons around the $(CHX)_i$ photon (Eq. 5, $nbKDE_{Xi}^X$) is somewhat more challenging (34). In this case, because the i^{th} photon is centered in the middle of the function and is no longer stochastically distributed, KDE_{Xi}^X contributes a unit to the sum leading to density overestimation. Thus, the i^{th} photon's contribution should not be considered (Eq. 5, see the $k \neq i$). However, simply ignoring the i^{th} photon results in an underestimation of the density, and therefore, we add the contribution of the redistributed i^{th} photon along the burst by

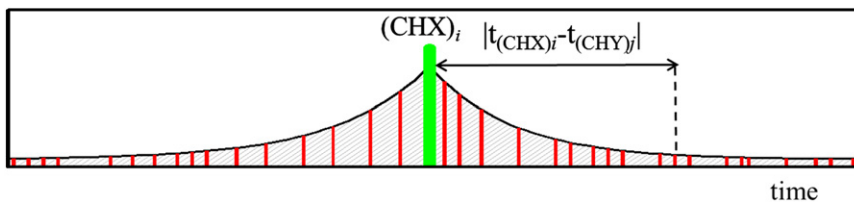


FIGURE 1 Schematic explanation of the kernel density estimator (KDE). (Green line, bold, centered) $(CHX)_i$ photon; (red lines, distributed, thin) channel-Y photons, and $t_{(CHX)_i}$ and $t_{(CHY)_j}$ are the arrival times of the $(CHX)_i$ and $(CHY)_j$ photons, respectively. Accordingly, KDE_{Xi}^Y calculates the total lengths of the red lines, e.g., a high channel-Y photon density around the $(CHX)_i$ photon results in a high value for KDE_{Xi}^Y .

multiplying by $1 + 2/N_{CHX}$. We empirically found that this small addition provides the most reliable estimation of the local density (data not shown):

$$nbKDE_{X_i}^X(t_{\{CHX\}}) = \left(1 + \frac{2}{N_{CHX}}\right) \times \sum_{k=1, k \neq i}^{N_{CHX}} \text{Exp} \left[-\frac{|t_{(CHX)_i} - t_{(CHX)_k}|}{\tau} \right]. \quad (5)$$

Accordingly, the nonbiased (nb) kernel density estimator ($nbKDE_{X_i}^X$) estimates the density of channel-X photons around the $(CHX)_i$ photon with a minor factor that fixes the bias caused by the i^{th} photon.

FRET-2CDE function

To calculate FRET-based 2CDE, we now define the donor channel (CHD) as channel-X and the acceptor channel (CHA) as channel-Y. Accordingly, based on Eqs. 4 and 5, which estimate the densities of the donor and acceptor photons, respectively, around the i^{th} photon (belonging to the donor-channel), Eq. 6 estimates the E values around each of the donor photons, summing all these estimated E values and dividing by the number of donor photons (N_{CHD}):

$$(E)_D = \frac{1}{N_{CHD}} \sum_{i=1}^{N_{CHD}} \frac{KDE_{D_i}^A}{KDE_{D_i}^A + nbKDE_{D_i}^D}. \quad (6)$$

As can be seen, E is calculated simply by dividing the density of acceptor photons by the sum of the acceptor's plus the donor's densities, similar to the conventional definition of E (Eq. 1). When FRET efficiency is fixed during the burst, $(E)_D$ converges to the averaged E (whereas a higher number of photons naturally reduces the statistical noise and yields better convergence). However, when the FRET efficiency is not fixed, periods with lower E values have higher donor photon densities, and hence, they are considered more frequently in the sum. This leads to the convergence of $(E)_D$ to values smaller than the averaged E , such convergence being a key element in FRET-2CDE function. In periods with low photon density, the denominator may equal zero (because photons are considered just up to $5 \times \tau$ before and after the central photon). Such cases are removed by the computer algorithm, and the N_{CHD} is reduced by a unit (explained in Fig. S1, but not reflected in either Eq. 6 or Eq. 7).

$$(1 - E)_A = \frac{1}{N_{CHA}} \sum_{j=1}^{N_{CHA}} \frac{KDE_{A_j}^D}{KDE_{A_j}^D + nbKDE_{A_j}^A}. \quad (7)$$

Here, similar to Eq. 6, which is based on donor photons, Eq. 7 estimates the $1-E$ values around each of the acceptor

photons, sums all the estimated $1-E$ values, and divides the result by the number of acceptor photons (N_{CHA}). Notice that $1-E$ is calculated based on dividing donor photon density by the sum of densities and not simply by calculating E and subtracting it from a unit. When FRET efficiency is fixed, $(1-E)_A$ converges to the average $1-E$ value, but when FRET efficiency is not fixed, periods with higher FRET values and relatively higher densities of acceptor photons are considered more frequently, resulting in $(1-E)_A$ convergence to values smaller than the averaged $1-E$.

$$\text{FRET} - 2\text{CDE}(t_{\{CHD\}}, t_{\{CHA\}}) = 110 - 100 \times [(E)_D + (1 - E)_A]. \quad (8)$$

Here, Eq. 8 shows the final form of the FRET-2CDE function, where we sum Eq. 6 and Eq. 7, multiply the sum by 100, and subtract the result from 110 (to achieve a convenient distribution of the calculated FRET-2CDE values). According to the channel definition given before, the left side of the equation inside the brackets calculates the averaged E around the donor photons whereas the right side calculates the averaged $1-E$ around the acceptor photons. Therefore, the sum inside the brackets converges to 1 when FRET is fixed (10 for the full FRET-2CDE function) and to values smaller than 1 when FRET is not fixed (higher than 10 for the full FRET-2CDE function).

ALEX-2CDE requirements and function

Whereas, when calculating FRET-2CDE we aim to maintain independence of the function on burst size and duration, in ALEX-2CDE we partially sacrifice these properties to achieve increased sensitivity to the brightness ratio distribution, thereby promoting the removal of unwanted subpopulations. Three modifications make the difference.

First, in contrast to the FRET-2CDE estimator, here we do not fix the bias formed by the inclusion of the i^{th} photon when calculating the local density of photons of the same channel, as in Eq. 5:

$$KDE_{X_i}^X(t_{\{CHX\}}) = \sum_{k=1}^{N_{CHX}} \text{Exp} \left[-\frac{|t_{(CHX)_i} - t_{(CHX)_k}|}{\tau} \right]. \quad (9)$$

As a result, $KDE_{X_i}^X$ overestimates the density of channel-X photons around the channel-X i^{th} photon. This overestimation is more profound in bursts with small numbers of photons in the examined channel.

Second, obviously, for calculating ALEX-based 2CDE, we define the photons detected during donor laser on-time (CHD_{EX}) as channel-X and those detected during the acceptor laser on-time (CHA_{EX}) as channel-Y.

Third, the modification regarding the FRET-2CDE estimator is that, based on Eqs. 4 and 9, we calculate

the acceptor/donor brightness ratio around each of the (CHD_{EX}), sum all the estimated ratios, and divide by the number of photons in CHA_{EX} ($N_{CHA_{EX}}$):

$$BR_{D_{EX}} = \frac{1}{N_{CHA_{EX}}} \sum_{i=1}^{N_{CHD_{EX}}} \frac{KDE_{D_{EX}^i}^{A_{EX}}}{KDE_{D_{EX}^i}^{D_{EX}}}. \quad (10)$$

Because the burst duration is equal for the two channels, when the brightness ratio is fixed along the burst, the part inside the sum converges to $N_{CHA_{EX}}/N_{CHD_{EX}}$, and it is summed $N_{CHD_{EX}}$ times and then divided by $N_{CHA_{EX}}$, resulting in the convergence of $BR_{D_{EX}}$ to 1. Note that $BR_{D_{EX}}$ does not calculate the average brightness ratio, which requires division by $N_{CHD_{EX}}$ instead of by $N_{CHA_{EX}}$. However, when the brightness ratio is not fixed, periods with relatively higher CHD_{EX} density ($N_{CHA_{EX}}/N_{CHD_{EX}}$ smaller than the average) are considered more frequently by Eq. 10, leading to the convergence of $BR_{D_{EX}}$ to values <1 , a key element in the ALEX-2CDE function. Similarly, we calculate the opposite brightness ratio (D/A instead of A/D) around the CHA_{EX} photons:

$$BR_{A_{EX}} = \frac{1}{N_{CHD_{EX}}} \sum_{j=1}^{N_{CHA_{EX}}} \frac{KDE_{A_{EX}^j}^{D_{EX}}}{KDE_{A_{EX}^j}^{A_{EX}}}. \quad (11)$$

When the brightness ratio is fixed, $BR_{A_{EX}}$ converged to 1, but when the ratio is not fixed, $BR_{A_{EX}}$ converged to values <1 .

$$\begin{aligned} & ALEX - 2CDE(t_{\{CHD_{EX}\}}, t_{\{CHA_{EX}\}}) \\ & = 100 - 50 \times [BR_{D_{EX}} + BR_{A_{EX}}]. \end{aligned} \quad (12)$$

Here, we sum Eqs. 10 and 11, multiply by 50, and subtract the result from 100 (for convenience). The expression inside the brackets converges to 2 (0 for the ALEX-2CDE) or to values <2 (>0 for the ALEX-2CDE) for fixed and not-fixed brightness ratios, respectively.

RESULTS AND DISCUSSION

Numeric simulations

Single-molecule FRET and ALEX experiments are complex to analyze due to the many different experimental parameters involved and to the nontrivial nature of molecule trajectories, burst intensities, and any burst search algorithm. Therefore, it is now common (18,19) to use numerical simulations to study the effects of experimental parameters on the acquired results.

FRET-2CDE filter reveals dynamics

To begin, we used simulation to demonstrate that the FRET-2CDE function can distinguish between bursts with fixed and fluctuating FRET, and as a result, it can help reveal underlying molecular dynamics. We simulated a scenario of static heterogeneity comprising an equimolar mixture of static species (Fig. 2 A, $E = 0.25, 0.35, 0.45, 0.55$,

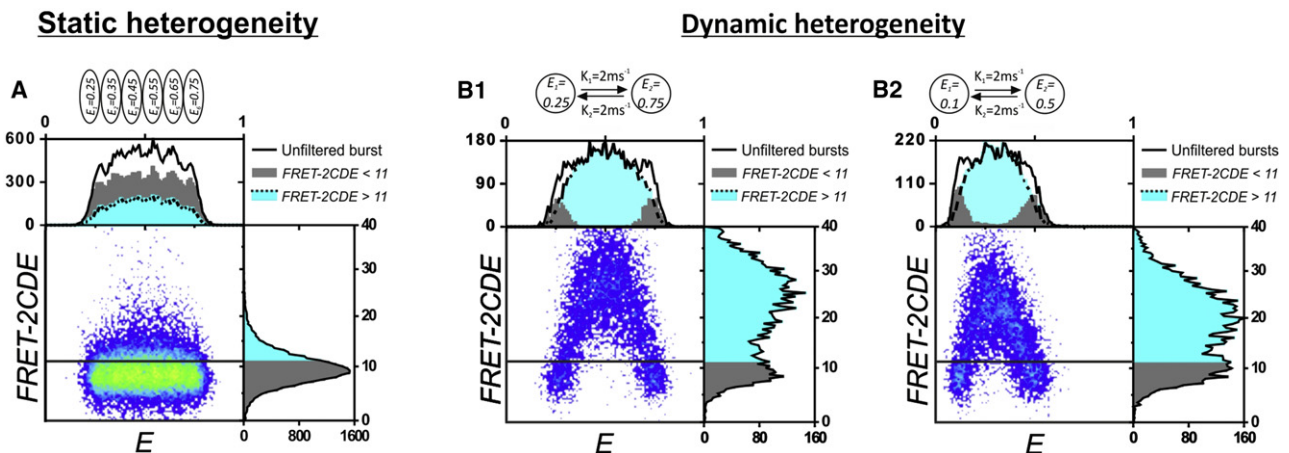


FIGURE 2 Demonstrations of FRET-2CDE estimator ability to differentiate static from dynamic heterogeneity and to reveal the underlying dynamics; E/FRET-2CDE one- and two-dimensional histogram representation of simulated data. Equimolar mixture of static species with $E = 0.25, 0.35, 0.45, 0.55$, and 0.65 (A), two-state model species with $E_1 = 0.25, E_2 = 0.75$, and $k_1 = k_2 = 2 \text{ ms}^{-1}$ (B1), and a two-state model species with $E_1 = 0.1, E_2 = 0.5$, and $k_1 = k_2 = 2 \text{ ms}^{-1}$ (B2). E and FRET-2CDE one-dimensional histograms of unfiltered bursts (black solid line) and of bursts with FRET-2CDE < 11 and > 11 (gray and cyan graphs, the latter is smaller and dotted with black lines) are presented. The static mixture was chosen such that its unfiltered FRET histogram would be undistinguishable from that of the dynamic species. Keeping bursts with FRET-2CDE < 11 (the portion under the horizontal line in the two-dimensional histograms) and rejecting those with FRET-2CDE > 11 reveals the striking differences between the static and the dynamic heterogeneity scenarios (gray in the E-histogram and located far from the histogram center). Most of the bursts in the static sample have FRET-2CDE ~ 10 , whereas a minority have values > 11 . In contrast, in the dynamic model, some events showed no change in FRET efficiency during the transient time, resulting in FRET-2CDE < 11 , whereas others experienced one or more FRET transitions that resulted in FRET-2CDE > 11 . The histogram in B2 demonstrates that the FRET-2CDE estimator is just weakly dependent on the averaged FRET efficiency.

0.65) and a scenario of dynamic heterogeneity where a species fluctuated between two FRET values in a two-state fashion (Fig. 2 B, $E_1 = 0.25$, $E_2 = 0.75$, $k_1 = k_2 = 2 \text{ ms}^{-1}$). To emphasize that the FRET-histogram alone does not always provide sufficient information for resolving the molecular dynamics and that further analysis is required, we chose the parameters such that the resultant FRET histograms (Fig. 2 A, B1, *solid black line* in the *E*-histograms) are (almost) identical. To identify the two scenarios and their underlying dynamical differences, we calculated the FRET-2CDE value for each burst and placed the results in an *E*/FRET-2CDE histogram.

As is clearly evident, the static scenario, in which no burst experiences a change in FRET (Fig. 2 A, *two-dimensional histogram* and *solid line* in the *FRET-2CDE one-dimensional histogram*), yielded FRET-2CDE values that were mainly < 11 , whereas the dynamic scenario (Fig. 2, B1 and B2), in which some bursts experienced changes in FRET during the transient time whereas others did not, yielded FRET-2CDE values ranging from ~ 0 to > 40 . To further emphasize the difference and to reveal the underlying dynamics, we used the FRET-2CDE function as a filter. The FRET histogram split between bursts with $FRET-2CDE < 11$ and > 11 (Fig. 2, *gray* and *cyan histograms*, respectively). In the static scenario, there was no significant difference between the shapes of the two histograms. However, in the dynamic scenario, $FRET-2CDE < 11$ yielded a FRET histogram containing two subpopulations revealing the two underlying states fairly accurately (Fig. 2. B1, $E_1 = 0.26$, $E_2 = 0.74$, fitting not shown), whereas $FRET-2CDE > 11$ yielded a very broad peak centered on $E = 0.5$. To demonstrate the function's weak dependence on the average E , we simulated a scenario with different E values (Fig. 2 B2, $E_1 = 0.1$, $E_2 = 0.5$, $k_1 = k_2 = 2 \text{ ms}^{-1}$). As can be seen, the five static subpopulations in Fig. 2 A and the static subpopulations in Fig. 2, B1 and B2, indeed yielded almost identical FRET-2CDE values.

ALEX-2CDE filter removes donor- and acceptor-only subpopulations and subpopulation mixing

Similarly, let us demonstrate that the ALEX-2CDE can distinguish between bursts with fixed and fluctuating brightness ratios, and as a result, it is capable of removing subpopulation mixing, donor-only and acceptor-only subpopulations, and dye bleaching and blinking events. We simulated the following mixture: 90 pM of donor-only species, 90 pM of acceptor-only species, and 3 pM each of four different doubly labeled species of interest we wish to identify (Fig. 3, A and B, $E = 0.25/S = 0.25$, $E = 0.75/S = 0.25$, $E = 0.25/S = 0.75$, and $E = 0.75/S = 0.75$). The 192-pM concentration of the mixture is fairly high for single-molecule experiments because more than one species is frequently present simultaneously in the confocal spot. As can be seen in Fig. 3 A, due to subpopulation mixing, bridges between subpopulations formed (especially between the highly concentrated donor- and acceptor-only subpopulations), thereby concealing the species of interest. To reveal these species, we calculated the ALEX-2CDE value for each burst (Fig. 3 C) and plotted the *E*/*S* histogram of bursts for which $ALEX-2CDE < 4$ (Fig. 3 C, *mark by arrow*, and D). The ALEX-2CDE filter successfully removed the donor- and acceptor-only subpopulations and most of the mixed subpopulations while maintaining enough bursts to enable identification of the four species of interest.

EXPERIMENTAL RESULTS

ALEX- and FRET-based 2CDE filters partially resolve hairpin dynamics

To experimentally demonstrate the benefits of using the FRET-2CDE estimator to identify structural dynamics, we chose the DNA hairpin as a source of FRET efficiency

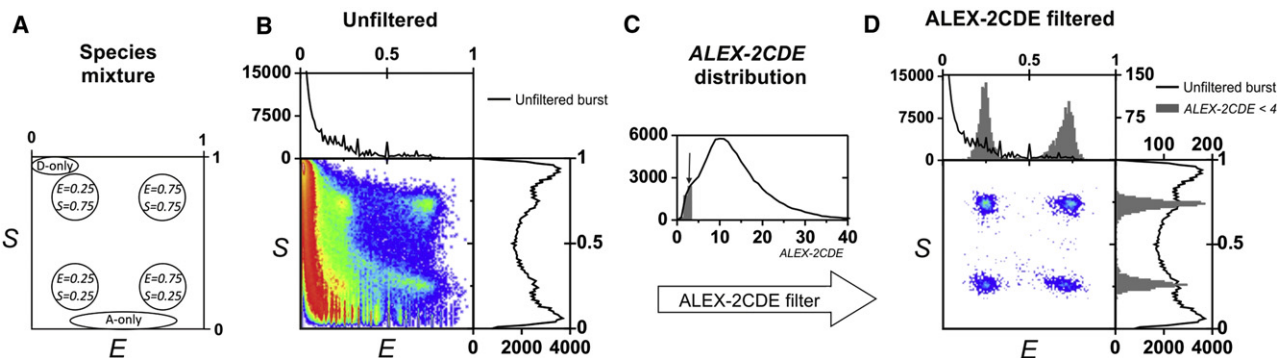


FIGURE 3 Demonstration of the ability of the brightness-ratio based ALEX-2CDE filter to remove donor- and acceptor-only subpopulations and subpopulation mixing. (A and B) Unfiltered *E*/*S* histogram generated from simulations of a mixture of several fluorescence species: 90 pM of donor-only molecule, 90 pM of acceptor-only molecule, and 3 pM of doubly labeled molecule with $E = 0.25/S = 0.25$, $E = 0.75/S = 0.25$, $E = 0.25/S = 0.75$, and $E = 0.75/S = 0.75$. (C) The ALEX-2CDE distribution of the unfiltered burst (*arrow* indicates $ALEX-2CDE = 4$). (D) *E*/*S* histogram of burst with $ALEX-2CDE < 4$. The *E* and *S* one-dimensional histograms (*gray*) of the filtered subpopulation are blown up relative to that of the unfiltered subpopulation. As can be seen, the ALEX-2CDE filter successfully removed the donor- and acceptor-only subpopulations and the mixing events and exposed the four subpopulations of interest.

fluctuations. The hairpin is designed to behave like a quasi-two-state model having high and low FRET values corresponding to the closed and open states, respectively (35,36). Two systems are presented; a freely diffusing hairpin (with a stamp sequence, TTGGT) and a somewhat slower, interconverting hairpin (stamp sequence elongated by a single G, TTGGGT) attached to a freely diffusing DNA origami (Fig. 4, A1–A4 and B1–B4, respectively). Because the origami is much larger in size than the hairpin, diffusion of the former is ~ 10 -times slower (as apparent from burst duration distribution, data not shown), thus providing a larger time window for the slower hairpin to fluctuate.

We performed a conventional FRET-ALEX experiment, calculated the E , S , $FRET-2CDE$, and $ALEX-2CDE$ for each burst, and placed the resultant E/S in a two-dimensional histogram. In the case of the freely diffusing hairpin, a major subpopulation of photoactive donors and acceptors and two minor subpopulations of donor- and acceptor-only were observed (Fig. 4 A2, S values at ~ 0.5 , 1, and 0, respectively). The latter group could comprise unhybridized ssDNA or singly labeled dsDNA or doubly labeled but bleached dye dsDNA. We therefore began by applying the

ALEX-2CDE filter to remove these subpopulations (Fig. 4 A3, $ALEX-2CDE < 10$). The remaining doubly labeled hairpin subpopulation showed a broad E distribution spanning from $\sim E = 0.3$ to $\sim E = 0.95$. We tested whether the hairpin indeed behaved like a quasi-two-state model using the FRET-2CDE filter by plotting one E/S histogram of bursts with $FRET-2CDE < 15$ and another with $FRET-2CDE > 15$ (Fig. 4 A4, gray and cyan, respectively). The former histogram has only two peaks located at $\sim E = 0.47$ and $E = 0.88$ (fitting not shown); no third intermediate is observed. These two peaks are events that did not experience FRET fluctuation during the transient time, assigned to the hairpins' open and closed states, thus suggesting that the hairpin indeed behaves according to a quasi-two-state model on the diffusion timescale.

We further tested the filter on the hairpin-origami sample (Fig. 4, B1–B4). Donor- and acceptor-only subpopulations were removed by the ALEX-2CDE filter (Fig. 4 B2, $ALEX-2CDE < 10$). Although the hairpin fluctuates fairly slowly, the long burst durations caused by the origami slow-diffusion enable state transitions during the transient through the confocal, resulting in a broad FRET distribution. Applying the FRET-2CDE estimator revealed two

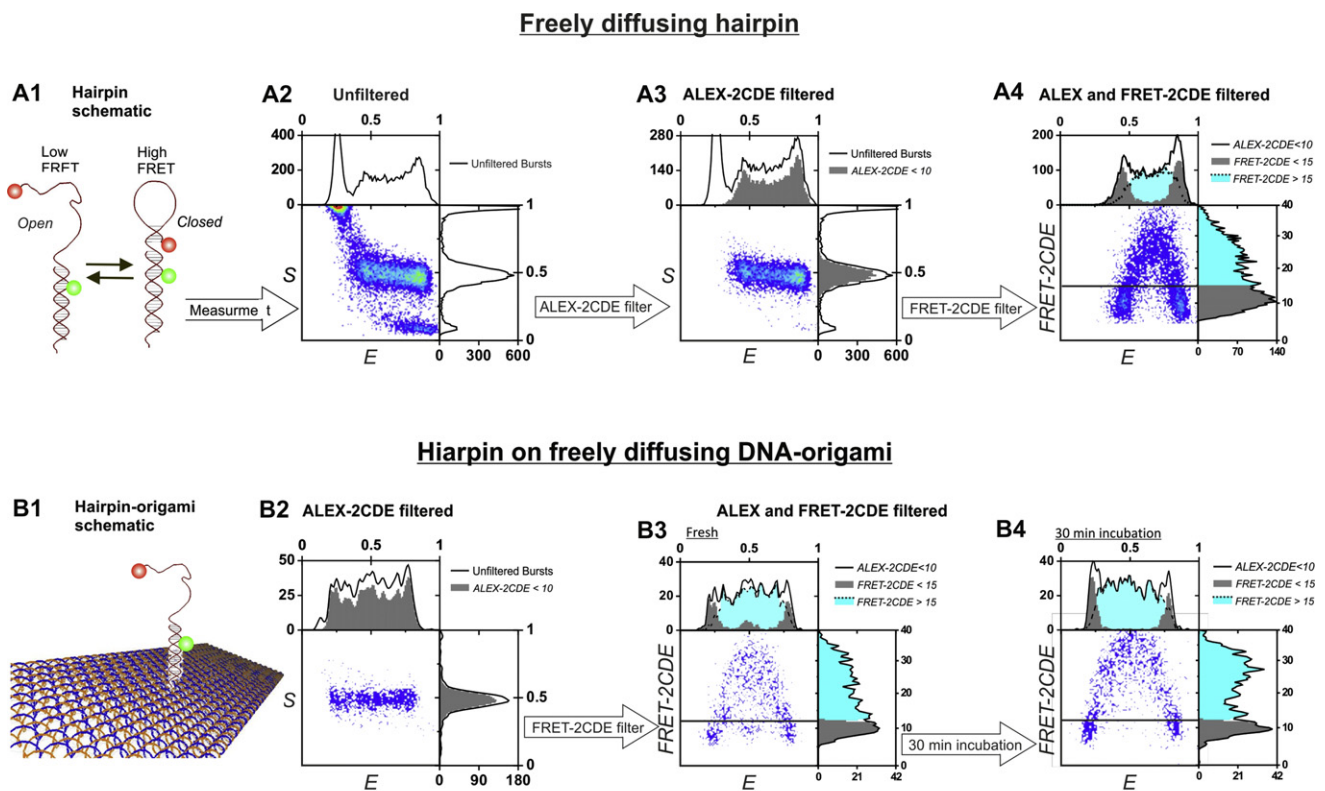


FIGURE 4 Experimental demonstration of the abilities of FRET-based 2CDE filters to identify structural dynamics and minor hidden subpopulations of freely diffusing two-state DNA-hairpin (A) and two-state DNA-hairpin attached to freely diffusing DNA origami (B). Schematic presentation of free hairpin and hairpin-origami (A1 and B1, respectively). (A2) Unfiltered data contain doubly labeled hairpin, and donor- and acceptor-only subpopulations. By choosing burst having $ALEX-2CDE < 10$, the donor- and acceptor-only subpopulations are removed (A3 and B2). Applying FRET-2CDE filter and plotting histogram of burst with $FRET-2CDE < 15$ and $FRET-2CDE > 15$ (A4, gray histogram, and B3 and B4, cyan histogram, respectively) reveals the hairpins underlying structure and their quasi-two-state nature.

peaks in the lower FRET-2CDE values (Fig. 4 B3, $FRET-2CDE < 15$) and, to our surprise, a third peak centered on $E = 0.5$. After incubating the sample for 30 min in the measurement concentration (3 pM) and remeasuring, the third subpopulation disappeared (Fig. 4 B4). More measurements are required to conclude the source of the third subpopulation, which is most probably stacking of two hairpins, which unfold at picomolar concentration. The unambiguous observation of a subpopulation, $<5\%$ of the total population, using the FRET-2CDE, however, demonstrates the ability of the estimator to identify and isolate subpopulations that would otherwise remain hidden in the greater ensemble.

ALEX-2CDE filters experimentally uncover hidden subpopulations

To experimentally demonstrate the ability of ALEX-2CDE to uncover minor (37) subpopulations hidden among high concentrations of foreign populations, we performed two sets of experiments.

In the first set of experiments (Fig. 5) mimicking affinity measurements (14), we mixed 30 pM of donor-labeled and 30 pM of acceptor-labeled ssDNA with 6 pM each of three different doubly labeled dsDNA (Fig. 5, A and B, $E = 0.22$, $E = 0.46$, and $E = 0.85$). The E/S histogram of the unfiltered data shows that the dsDNA subpopulations are almost completely concealed by the bridges that resulted from subpopulation mixing. Applying the ALEX-2CDE filter (Fig. 5, C and D, $ALEX-2CDE < 4$) almost completely removed the donor- and acceptor-only subpopulations and the bridges, exposing the doubly labeled subpopulation.

The second set of experiments was part of our effort to measure DNA motor (32) activity (Fig. 6). A bipedal motor labeled with donor dye on one leg walked on a DNA origami

containing six footholds, three of which were labeled with acceptor dyes (Fig. 6, A1–A3). The intact subpopulation with its three acceptors and one donor was observed at $S = 0.25$, while the bipedal-only or origami-only (defective motors) subpopulations were observed at $S = 0.95$ and $S = 0.1$, respectively (Fig. 6, B and C), as expected. Sequences of fuel and anti-fuel were introduced from outside to encourage corresponding leg attachment to and detachment from the footholds, ultimately resulting in motor progress (Fig. 6, just five out of fifteen steps are schematically presented, in Fig. 6 A, and just three measurements are presented, Fig. 6, B and C). As the motor progressed, some bipedal motors disconnected from the origami, thereby decreasing the subpopulation of interest and increasing the acceptor-only and donor-only subpopulations. In the first step presented (Fig. 6 B1), the intact subpopulation was identified without the ALEX-2CDE filter, but in subsequent steps (Fig. 6, B2 and B3), the intact subpopulation was completely hindered by the acceptor-only subpopulation. Filtering the bursts using $ALEX-2CDE < 8$ removed donor- and acceptor-only subpopulations and mixing subpopulations and exposed the intact subpopulation (Fig. 6, C2 and C3), allowing analysis of the motor's acquired conformational state using the FRET histogram.

ALEX-2CDE filter removes bleaching and blinking events

Because the ALEX-2CDE filter is sensitive to fluctuations in the brightness ratio, it can identify and remove events in which donor or acceptor dyes bleach or blink. We simulated a species in which the acceptors stochastically bleach or blink (see Fig. S4). The unfiltered E/S histograms show a strong tail spanning from the nonbleached and nonblinked subpopulations toward the donor-only subpopulation as

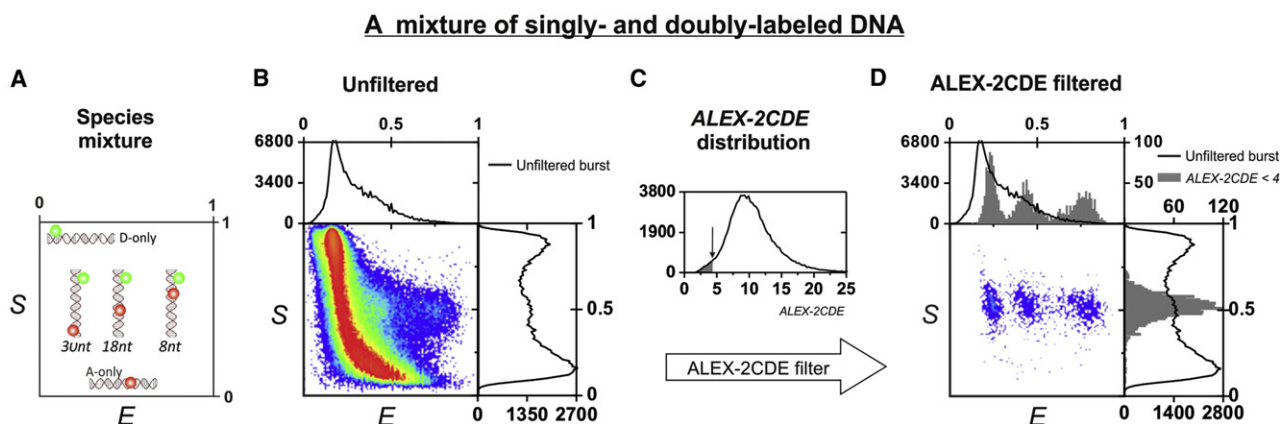


FIGURE 5 Experimental demonstrations of the ability of the ALEX-2CDE filter to uncover a minor, doubly labeled dsDNA subpopulation hidden in the larger concentrations of singly labeled dsDNA subpopulations. (A) Mixture of 30 pM donor-labeled and 30 pM acceptor-labeled ssDNA with three different doubly labeled dsDNA, 6 pM each ($E = 0.22$, $E = 0.46$, and $E = 0.85$). (B) The unfiltered data show that the dsDNA subpopulations are almost completely concealed by the bridges. Applying the ALEX-2CDE filter and choosing events with $ALEX-2CDE < 4$ (C and D) almost completely removed the donor- and the acceptor-only subpopulations and the bridges, exposing the doubly labeled subpopulation.

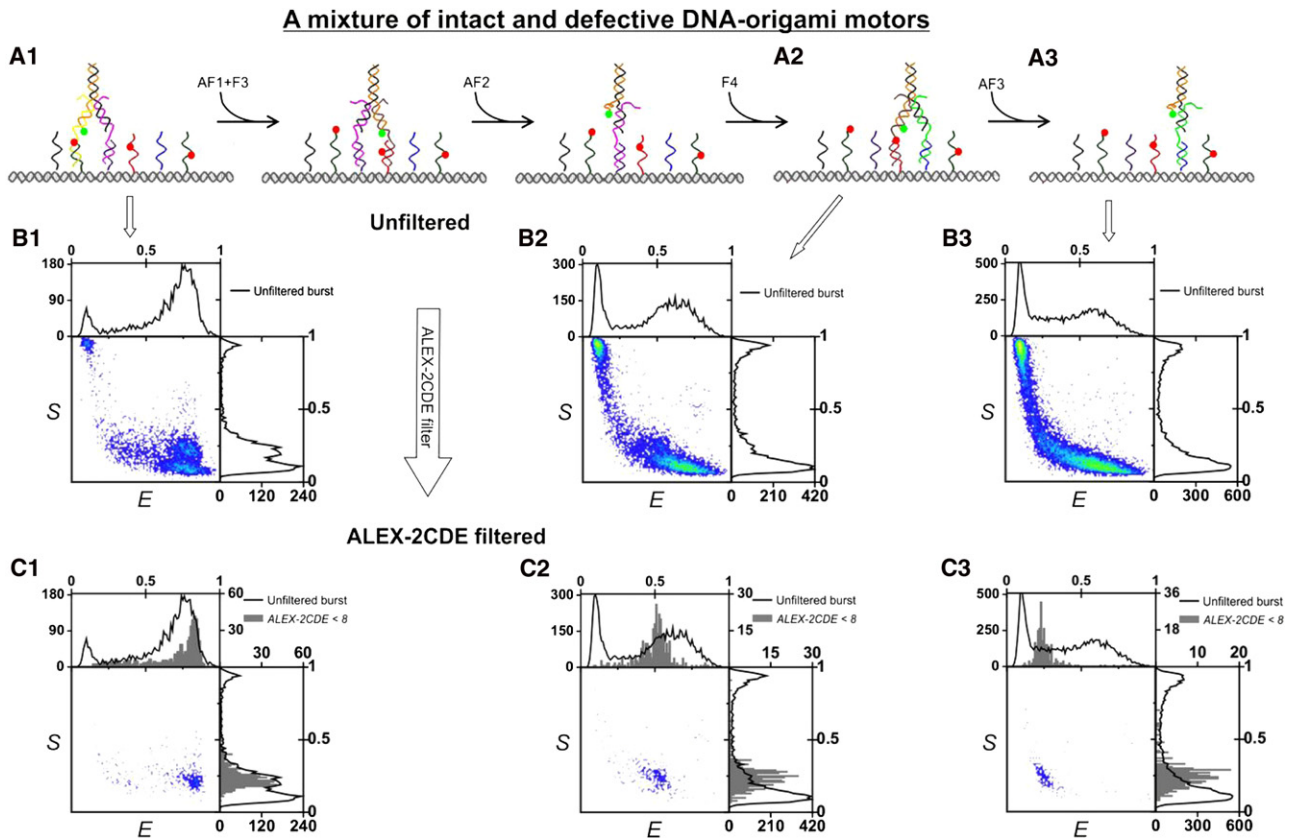


FIGURE 6 Experimental demonstrations of the ability of the ALEX-2CDE filter to uncover minor intact origami motors concealed by a high concentration of defective motors. (A) Schematic presentation of five out of fifteen motor-striding steps upon addition of fuel and anti-fuel. Unfiltered data (B1–B3) and ALEX-2CDE based filtered data (C1–C3) are presented. As the reaction progressed (A1–A3), the intact subpopulation ($S = 0.25$) decreased and the defective subpopulations ($S = 0.1$ and $S = 0.9$) increased. Filtering for $ALEX-2CDE < 8$ exposed the intact subpopulation in their high, medium, and low FRET (C1–C3, blown-up gray histograms).

expected. To remove the tails, we plotted the E/S histogram of bursts having $ALEX-2CDE < 10$ (see Fig. S4, A2 and B2), and the ALEX-2CDE filter removed most of the bleaching and blinking events, maintaining enough bursts to recover the nonbleached and nonblinked subpopulations.

FRET-2CDE estimator dependence on burst size, rates, E differences and E values

The FRET-2CDE estimator is designed to enable the identification of events that either contain or lack dynamics, independently of burst size and burst mean E . To demonstrate this independence, we compared the FRET-2CDE distributions of five simulated species (see Fig. S5 A1, $E = 0.1, 0.3, 0.5, 0.7, 0.9$). The burst size distributions of the five species were equal (data not shown), but the relative intensities of the donor and acceptor channels were varied to achieve the five mean E values. As can be seen, there were no major differences in the FRET-2CDE distributions, and as a result, filtering the populations based on FRET-2CDE scores (here, $FRET-2CDE < 11$) maintained the relative abundance of each species, as desired. A minimal dependence on burst size is evident in Fig. S5 A2. (For

a more detailed compression of the dependent of FRET-2CDE distribution on burst size, interconversion rates, FRET efficiency differences, and FRET efficiency values, see Fig. S6, Fig. S7, Fig. S8, and Fig. S9.) Based on these comparisons, users can estimate the expected FRET-2CDE distribution for broad spectrum of bursts intensities and dynamical scenarios. In contrast to BVA (25), where the per-burst standard deviation depends on mean E , here the FRET-2CDE distributions of bursts of varying size, despite their varying widths due to reasons associated with shot-noise, were all centered on $FRET-2CDE = 10$, as desired.

ALEX-2CDE estimator dependence on S , and burst size

Slightly different from the FRET-2CDE estimator, the ALEX-2CDE is designed to serve as a filter capable of removing events containing brightness ratio fluctuations while devoting less attention to independence of the mean S . We compared the ALEX-2CDE distributions of seven simulated species: five doubly labeled species and one donor-only and acceptor-only subpopulation each (see

Fig. S5 B1, $S = 0.1, 0.3, 0.5, 0.7,$ and 0.9). The burst size distributions of the seven species were identical (data not shown), but their intensities were divided unequally between the two channels to achieve various S values. The species with intermediate S values ($0.3, 0.5,$ and 0.7), where the two channels contained relatively high numbers of photons, yielded ALEX-2CDE distributions centered on 2.5. The peripheral S values (0.1 and 0.9), where one channel contained a small number of photons, yielded somewhat higher values centered on 5. The donor- and acceptor-only subpopulations, where one of the channels was very weak, yielded much higher values centered at ~ 30 . Unlike those for FRET-2CDE, the ALEX-2CDE distributions increased as burst sizes decreased (see **Fig. S5 B2**), a result of calculating BR_{DEX} and BR_{AEX} via division by the biased KDE and not the nonbiased $nbKDE$ (Eqs. 10 and 11). As a result, when one (or both) of the channels was weak, e.g., the channel- X KDE_{Xi}^X was overestimated, the BR_X was underestimated, leading to larger values for ALEX-2CDE.

Influence of τ on 2CDE estimators

Both the KDE and nbKDE functions have the same role—to estimate local photon density by overcoming the stochastic nature of photon arrival time. Thus, although on the one hand, τ must be as small as possible for estimations of local density, on the other hand, if τ is too small the estimated density will be too noisy. Several methods, based on cross-validation and a plug-in rule, of calculating the best τ were suggested (34). The general recommendation is to decrease τ as much as the stochastic noise allows. Indeed, we found that the 2CDE estimators performed better with a relatively small τ , and the quality of the 2CDE estimators was only weakly dependent on τ as long as it was kept small (see **Fig. S10**). Therefore, although we recommend tuning τ to achieve the best filter performance, small values of τ (30 – $500 \mu s$) are usually suitable for analyzing typical single-molecule data.

Using 2CDE as an estimator and filter

Excluding τ and the properties of interest—FRET and brightness ratio distributions—the 2CDE was intentionally designed to be independent of, or only weakly dependent on, many experimental factors or preassumed theoretical models. As such, 2CDE can be directly implemented on the data and then used as an estimator, which reflects the FRET or brightness ratio distribution, or as a filter, which removes subpopulations. In the latter case, if possible, the threshold should be chosen such that it satisfies the experimental needs (e.g., removing mixing) while maintaining enough events that belong to the subpopulations of interest. If the number of events after the filtering is too small, we recommend taking a longer measurement.

Using FRET-2CDE to resolve dynamics

The FRET-2CDE estimator is capable of identifying and isolating events that lack dynamics, and in so doing it can reveal the underlying structure (e.g., the two states of the hairpins). This structural information can be further used to increase the reliability of the current PDA methods (20–25) by fixing the structural parameters (the states) and leaving the dynamic parameters (rates) free for fitting. Our method can be further expanded to analyze and resolve dynamics in a manner similar to the recently developed BVA method (25), but this requires a more rigorous theoretical framework that is beyond the scope of this article. Recently, a method was developed that extends the ability to identify and measure dynamics up to 50 ms by comparing sequential bursts and identifying events recurrence (38). Whereas this method reveals dynamics by comparing different bursts, our method examines the dynamics inside the burst, making them complementary methods.

CONCLUSIONS

We introduce what to our knowledge is a new approach for analyzing data collected in diffusion-based single-molecule FRET and FRET/ALEX experiments. It turns out that despite their limited number, the photon distributions in the various channels of the bursts carry enough information to enable, based on properties of interest, burst classification beyond what is possible using only mean values. In particular, we look for the FRET and brightness ratio distributions along the burst. The former is used to identify dynamics and to filter events with dynamics from those without, thus exposing the underlying structure of a quasi-two-state hairpin. The latter is used to identify and remove events that exhibit brightness ratio distributions, which facilitates the exposure of minor doubly labeled dsDNA hidden in higher concentrations of singly labeled dsDNA and the exposure of functioning DNA origami motors concealed in a larger concentration of defective motors.

The approach we propose here has three benefits: 1), its ability to report on the presence/absence of dynamics and the underlying conformational states; 2), its ability to remove mixing, blinking, bleaching, and donor- and acceptor-only events facilitates the more reliable and accurate collection of data and enables conducting the experiment at higher concentrations; and 3), its increase in the ability to observe minor static or dynamic subpopulations that would otherwise be hidden in the greater hydrogenous ensemble. The 2CDE estimators are, by design, minimally dependent on the stochastic natures of photon emission and molecular diffusion, and therefore, they provide typical and understandable distributions and robust criteria for filtering. The estimators are ready-to-use, and as such, there is no need for additional theoretical framework or models or control experiments. The method can be expanded to identify other

interesting physical properties, such as the number of FRET or brightness transition occurring during the burst, and it can be extended for three-color ALEX. Our method can be fused with MFD (13), with RASP (38), and with BVA (25), to provide a more complete and robust method for structural dynamics analysis of individual biomolecules.

SUPPORTING MATERIAL

One table and nine figures are available at [http://www.biophysj.org/biophysj/supplemental/S0006-3495\(11\)05464-6](http://www.biophysj.org/biophysj/supplemental/S0006-3495(11)05464-6).

The authors thank O. Krichevsky for kindly providing access to his high performance liquid chromatography and 532-nm laser.

REFERENCES

- Roy, R., S. Hohng, and T. Ha. 2008. A practical guide to single-molecule FRET. *Nat. Methods*. 5:507–516.
- Wozniak, A. K., G. F. Schröder, ..., F. Oesterheld. 2008. Single-molecule FRET measures bends and kinks in DNA. *Proc. Natl. Acad. Sci. USA*. 105:18337–18342.
- Birkedal, V., M. Dong, ..., J. Kjems. 2011. Single molecule microscopy methods for the study of DNA origami structures. *Microsc. Res. Tech.* 74:688–698.
- Stein, I. H., V. Schüller, ..., T. Liedl. 2011. Single-molecule FRET ruler based on rigid DNA origami blocks. *Chem. Phys. Chem.* 12:689–695.
- Goodman, R. P., M. Heilemann, ..., A. J. Turberfield. 2008. Reconfigurable, braced, three-dimensional DNA nanostructures. *Nat. Nanotechnol.* 3:93–96.
- Jungmann, R., C. Steinhauer, ..., F. C. Simmel. 2010. Single-molecule kinetics and super-resolution microscopy by fluorescence imaging of transient binding on DNA origami. *Nano Lett.* 10:4756–4761.
- Deniz, A. A., and A. C. M. Ferreon. 2011. Protein folding at single-molecule resolution. *Biochim. Biophys. Acta Proteins Proteom.* 1814:1021–1029.
- Schuler, B., and W. A. Eaton. 2008. Protein folding studied by single-molecule FRET. *Curr. Opin. Struct. Biol.* 18:16–26.
- Chung, H. S., J. M. Louis, and W. A. Eaton. 2009. Experimental determination of upper bound for transition path times in protein folding from single-molecule photon-by-photon trajectories. *Proc. Natl. Acad. Sci. USA*. 106:11837–11844.
- Chung, H. S., I. V. Gopich, ..., W. A. Eaton. 2011. Extracting rate coefficients from single-molecule photon trajectories and FRET efficiency histograms for a fast-folding protein. *J. Phys. Chem. A*. 115:3642–3656.
- Gansen, A., A. Valeri, ..., C. A. Seidel. 2009. Nucleosome disassembly intermediates characterized by single-molecule FRET. *Proc. Natl. Acad. Sci. USA*. 106:15308–15313.
- Kapanidis, A. N., E. Margeat, ..., R. H. Ebricht. 2006. Initial transcription by RNA polymerase proceeds through a DNA-scrunching mechanism. *Science*. 314:1144–1147.
- Sisamakidis, E., A. Valeri, ..., C. A. Seidel. 2010. Accurate single-molecule FRET studies using multiparameter fluorescence detection. *Methods Enzymol.* 475:455–514.
- Kapanidis, A. N., N. K. Lee, ..., S. Weiss. 2004. Fluorescence-aided molecule sorting: analysis of structure and interactions by alternating-laser excitation of single molecules. *Proc. Natl. Acad. Sci. USA*. 101:8936–8941.
- Müller, B. K., E. Zaychikov, ..., D. C. Lamb. 2005. Pulsed interleaved excitation. *Biophys. J.* 89:3508–3522.
- Hohng, S., C. Joo, and T. Ha. 2004. Single-molecule three-color FRET. *Biophys. J.* 87:1328–1337.
- Lee, N. K., A. N. Kapanidis, ..., S. Weiss. 2007. Three-color alternating-laser excitation of single molecules: monitoring multiple interactions and distances. *Biophys. J.* 92:303–312.
- Antonik, M., S. Felekyan, ..., C. A. Seidel. 2006. Separating structural heterogeneities from stochastic variations in fluorescence resonance energy transfer distributions via photon distribution analysis. *J. Phys. Chem. B*. 110:6970–6978.
- Nir, E., X. Michalet, ..., S. Weiss. 2006. Shot-noise limited single-molecule FRET histograms: comparison between theory and experiments. *J. Phys. Chem. B*. 110:22103–22124.
- Kalinin, S., S. Felekyan, ..., C. A. Seidel. 2007. Probability distribution analysis of single-molecule fluorescence anisotropy and resonance energy transfer. *J. Phys. Chem. B*. 111:10253–10262.
- Gopich, I. V., and A. Szabo. 2007. Single-molecule FRET with diffusion and conformational dynamics. *J. Phys. Chem. B*. 111:12925–12932.
- Gopich, I. V., and A. Szabo. 2009. Decoding the pattern of photon colors in single-molecule FRET. *J. Phys. Chem. B*. 113:10965–10973.
- Santoso, Y., J. P. Torella, and A. N. Kapanidis. 2010. Characterizing single-molecule FRET dynamics with probability distribution analysis. *Chem. Phys. Chem.* 11:2209–2219.
- Kalinin, S., A. Valeri, ..., C. A. Seidel. 2010. Detection of structural dynamics by FRET: a photon distribution and fluorescence lifetime analysis of systems with multiple states. *J. Phys. Chem. B*. 114:7983–7995.
- Torella, J. P., S. J. Holden, ..., A. N. Kapanidis. 2011. Identifying molecular dynamics in single-molecule FRET experiments with burst variance analysis. *Biophys. J.* 100:1568–1577.
- Gopich, I. V. 2008. Concentration effects in “single-molecule” spectroscopy. *J. Phys. Chem. B*. 112:6214–6220.
- Kong, X., E. Nir, ..., S. Weiss. 2007. Photobleaching pathways in single-molecule FRET experiments. *J. Am. Chem. Soc.* 129:4643–4654.
- Di Fiori, N., and A. Meller. 2010. The effect of dye-dye interactions on the spatial resolution of single-molecule FRET measurements in nucleic acids. *Biophys. J.* 98:2265–2272.
- Sabanayagam, C. R., J. S. Eid, and A. Meller. 2005. Long time scale blinking kinetics of cyanine fluorophores conjugated to DNA and its effect on Förster resonance energy transfer. *J. Chem. Phys.* 123:224708.
- Vogelsang, J., C. Steinhauer, ..., P. Tinnefeld. 2010. Make them blink: probes for super-resolution microscopy. *Chem. Phys. Chem.* 11:2475–2490.
- Rothmund, P. W. 2006. Folding DNA to create nanoscale shapes and patterns. *Nature*. 440:297–302.
- Shin, J.-S., and N. A. Pierce. 2004. A synthetic DNA walker for molecular transport. *J. Am. Chem. Soc.* 126:10834–10835.
- Cordes, T., J. Vogelsang, and P. Tinnefeld. 2009. On the mechanism of Trolox as antiblinking and antibleaching reagent. *J. Am. Chem. Soc.* 131:5018–5019.
- Sheather, S. J., and M. C. Jones. 1991. A reliable data-based bandwidth selection method for kernel density estimation. *J. Roy. Stat. Soc. B Met.* 53:683–690.
- Ying, L. M., M. I. Wallace, and D. Klenerman. 2001. Two-state model of conformational fluctuation in a DNA hairpin-loop. *Chem. Phys. Lett.* 334:145–150.
- Bonnet, G., O. Krichevsky, and A. Libchaber. 1998. Kinetics of conformational fluctuations in DNA hairpin-loops. *Proc. Natl. Acad. Sci. USA*. 95:8602–8606.
- Laurence, T. A., Y. Kwon, ..., D. Barsky. 2007. Correlation spectroscopy of minor fluorescent species: signal purification and distribution analysis. *Biophys. J.* 92:2184–2198.
- Hoffmann, A., D. Nettels, ..., B. Schuler. 2011. Quantifying heterogeneity and conformational dynamics from single molecule FRET of diffusing molecules: recurrence analysis of single particles (RASP). *Phys. Chem. Chem. Phys.* 13:1857–1871.